Orientationally Controlled Nanoporous Cylindrical Domains in Polystyrene-*b*-poly(ferrocenylethylmethylsilane) Block Copolymer Films

David A. Rider,[†] Kevin A. Cavicchi,[‡,⊥] Lawrence Vanderark,[†] Thomas P. Russell,*[,‡] and Ian Manners*[,§]

Department of Chemistry, University of Toronto, Toronto, Ontario, Canada M5S 3H6; Polymer Science and Engineering Department, University of Massachusetts, Amherst, Massachusetts 01003; and Department of Chemistry, University of Bristol, Bristol, UK BS8 1TS

Received September 6, 2006; Revised Manuscript Received January 22, 2007

ABSTRACT: The self-assembly of thin films of organometallic cylinder-forming amorphous polystyrene-*block*-polyferrocenylsilane diblock copolymers is described. By varying film thickness and/or the conditions of toluene during evaporation annealing, well-ordered arrays of hexagonally packed iron-rich cylindrical microdomains oriented either parallel to or normal to the substrate were produced. In the latter case, when the film thickness was very small (12−15 nm), well-defined nanoporous cylindrical domains were found. This unique morphology persists in UV ozone etched films where inorganic, ring-like cylindrical domains were produced. By varying the rate of solvent evaporation from solvent-swollen films, control over the orientation, order, and size of the cylindrical microdomains was achieved and variation of the fundamental morphology was observed.

Introduction

In the bulk, diblock copolymers self-assemble into well-ordered arrays of nanometer-sized microdomains provided χN is greater than a critical value.[1,2] Here, χ is the segmental interaction parameter and N is the total number of segments in the block copolymer. In thin films, these well-defined morphologies are of intense current interest for applications including porous membranes, lithographic templates, and photonic band-gap materials.[1,3,4] The morphologies, ranging from spherical to cylindrical to gyroid to lamellar, are accessible depending on the volume fraction of the components, ϕ, while N dictates the size.[5] Essential to the utilization of these versatile materials is the ability to control the orientation and lateral ordering of the microdomains. Recently, the annealing of thin films of block copolymers in solvent vapor, followed by a controlled evaporation rate of the solvent, has opened a new pathway to meet these demands.[6−11]

While much effort has focused on organic materials, block copolymers containing transition metals suggest additional functions due to their redox, photophysical, conductive, catalytic, or preceramic properties.[12−16] Polyferrocenylsilane (PFS, Scheme 1) block copolymers (BCP's) are of particular interest due to the iron atoms in the main chain.[17−19] In selective solvents these materials self-assemble into a range of micellar-type morphologies, including nanoscopic cylinders, vesicles, and nanotubes, which further expands their potential applications.[20−24] PFS−BCP's in the solid state microphase-separate into iron-rich nanodomains[20,25−31] and, in thin films, are attracting attention due to redox-induced morphology changes, as plasma etch-resistant nanotemplates and as precursors to magnetic or catalytic materials.[9,26,29,30,32−34] Until recently, the self-assembly of PFS−BCP's in thin films has focused on the symmetrically substituted poly(ferrocenyldimethylsilane) (PFDMS, Scheme 1, R = R′ = Me) which has been shown to be semicrystalline.[35−38] This feature can drive the morphologies in thin films into a nonequilibrium state, complicating morphological control.[29,34,39−47] Recently, we reported the synthesis and bulk self-assembly of amorphous polystyrene-*block*-poly(ferrocenylethylmethylsilanes) (PS-*b*-PFEMS, Scheme 2).[48] Preliminary studies on thin films of PS-*b*-PFEMS have shown that the block copolymer self-assembles into a cylindrical microdomain morphology with the PFEMS cylindrical microdomains oriented normal to the film surface.[9,49] It follows, therefore, that solvent vapor annealing of thin films of PS-*b*-PFEMS merits study where the control of the orientation and lateral ordering of the cylindrical microdomains is expected. We demonstrate these outcomes herein and show that, by controlling the rate of solvent evaporation in solvent-swollen thin films, a simple route to ring-like cylindrical domains is achieved.

Scheme 1

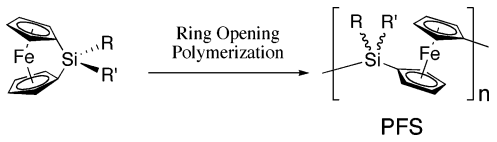

PFS

Scheme 2

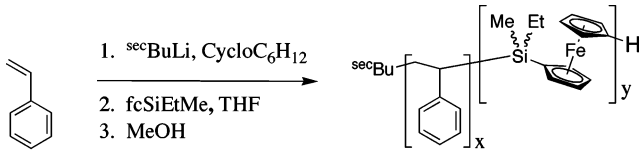

PS-*b*-PFEMS

Experimental Section

Equipment and Materials. Toluene was purified using a Grubbs-type solvent system. A polystyrene homopolymer (M_n = 29 300, PDI = 1.01) was used as received from Aldrich. Molecular weights were determined by gel permeation chromatography (GPC) using a Waters Associates liquid chromatograph equipped with a Waters 410 differential refractometer and a Viscotek T60A dual

[†] University of Toronto.
[‡] University of Massachusetts.
[§] University of Bristol.
[⊥] Current address: Department of Polymer Engineering, University of Akron, Akron, OH 44325.

10.1021/ma062073u CCC: $37.00 © 2007 American Chemical Society
Published on Web 04/21/2007

Table 1. Molecular Characteristics of Polymers Used in This Study

polymer	M_n[a]	M_w[b]	M_w/M_n[c]	ϕ_{PS}[d]	ϕ_{PFEMS}[d]	x[e]	y[d]
PS	29 300	29 600	1.01	1	0	281	0
PFEMS	10 000	10 100	1.01	0	1	0	39
PS-*b*-PFEMS (0.25)	38 700	38 700	1.00	0.75	0.25	263	44
PS-*b*-PFEMS (0.36)	68 200	70 900	1.04	0.64	0.36	389	108

[a] For block copolymers, from PS aliquot sampled during synthesis and ^{1}H NMR data. Standard deviation estimated to be ~5%. [b] For block copolymers, from PS aliquot sampled during synthesis, H NMR, and M_w/M_n data. [c] From GPC curve. Standard deviation estimated to be ~1%. [d] For block copolymers, from ^{1}H NMR integration and PS aliquot data. [e] For block copolymers, from PS aliquot sampled during synthesis.[48]

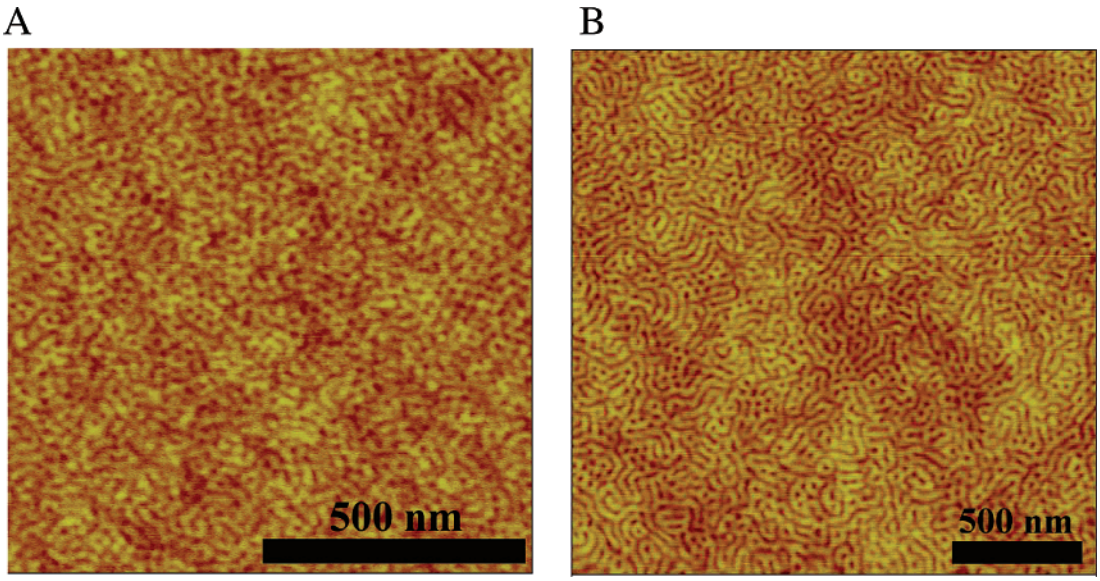

Figure 1. As-cast scanning force microscope height images of (A) PS-*b*-PFEMS (0.25) and (B) PS-*b*-PFEMS (0.36) (height scale = 10 nm).

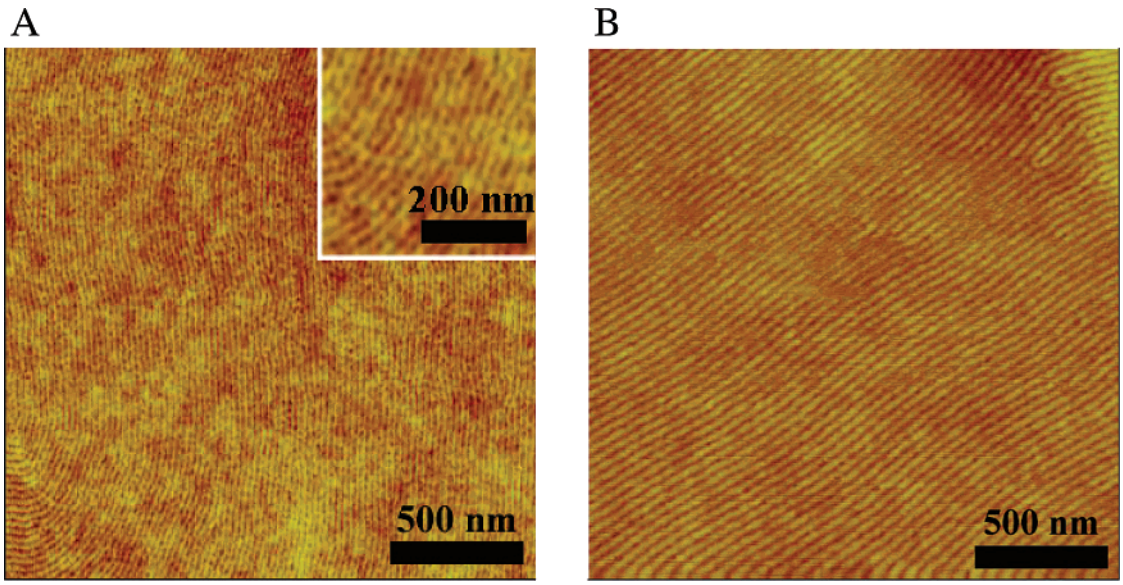

Figure 2. Height mode scanning force microscope images of toluene evaporation annealed (A) PS-*b*-PFEMS (0.25) and (B) PS-*b*-PFEMS (0.36) (height scale = 10 nm).

detector consisting of a 90° angle laser light scattering detector (λ_0 = 670 nm) and a four-capillary differential viscometer. Alternatively, molecular weights were determined using a Viscotek GPC MAX liquid chromatograph equipped with a Viscotek triple detector array. The triple detector array consists of a refractometer, a four-capillary differential viscometer, a 90° angle laser, and a low-angle laser (7°) light scattering detector (λ_0 = 670 nm). The triple-detector system has been shown to provide absolute M_w values for PFS homopolymers,[50] and we assume that it provides accurate values of M_w/M_n. In both cases, a flow rate of 1.0 mL/min was used with THF as the eluent. Film thicknesses were estimated using a Sopra (GES-5) spectroscopic ellipsometer with a multiwavelength light source (250−2000 nm) and an analyzer operated with the integration time for each data point being determined by either the minimum threshold of 2×10^6 detector counts or 10 s. A Levenberg−Marquardt regression algorithm was used to model the data as described previously.[51] Alternatively, film thicknesses were estimated using scanning force microscopy (SFM) of a scratched area. SFM, operated in tapping mode, was performed on a Multimedia Nanoscope IIIa SFM (Digital instrument/Veeco-Metrology Group). The SFM tips had resonant frequencies close to 170 kHz. Transmission electron microscopy (TEM) images were obtained using a Hitachi 600 electron microscope with an accelerating voltage of 75 kV. Small-angle X-ray scattering (SAXS) data

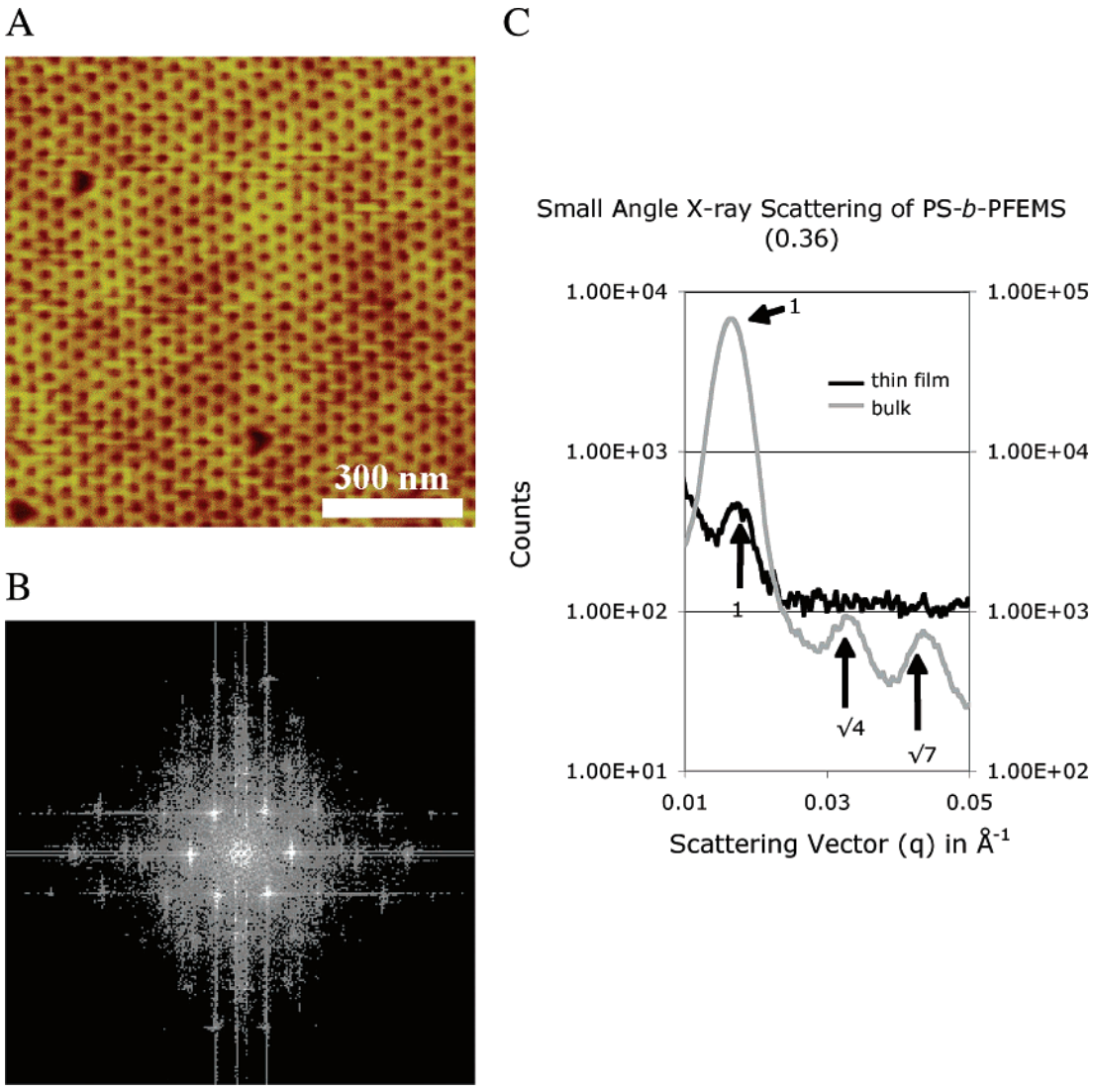

Figure 3. (A) Height image scanning force micrograph of saturated toluene evaporation annealed PS-*b*-PFEMS (0.36) thin film (height scale = 10 nm), (B) corresponding 2D Fourier transform, and (C) the small-angle X-ray scattering plots of PS-*b*-PFEMS (0.36) in the thin film (black trace) and the bulk state (gray trace).

were obtained using a Molecular Metrology instrument operated with a 2-dimensional gas-filled multiwire detector and 0.030 kW microsource X-ray tube with a confocal multilayer optic to produce a focused, monochromatic X-ray beam ($\lambda = 0.154$ nm). The scattering vector, q, was calibrated using silver behenate, and the sample-to-detector distance was 1.5 m. For thin film samples, the X-ray beam was passed through the silicon wafer and then the PS-*b*-PFEMS film. UV ozonolysis was performed using a SAMCO model UV-1 UV−ozone cleaning system operated with a oxygen flow rate of 0.5 L/min at 80 °C for 30 min.

Synthesis of a Poly(ferrocenylethylmethylsilane) Homopolymer and Polystyrene-*block*-poly(ferrocenylethylmethylsilane) (PS-*b*-PFEMS) Diblock Copolymers. The complete synthetic details concerning the synthesis of the PFEMS and PS-*b*-PFEMS materials used in this study have been published elsewhere.[48] The diblock copolymers used in this study were PS-*b*-PFEMS (0.25) and PS-*b*-PFEMS (0.36), where the value in parentheses denotes the volume fraction of PFEMS (ϕ_{PFEMS}). The former is composed of a PS segment of 27 400 g/mol and a PFEMS segment of 11 300 g/mol, whereas the latter contains a 40 500 g/mol PS segment and a 27 700 g/mol PFEMS segment. The respective polydispersity indices were 1.00 and 1.04 as determined by gel permeation chromatography equipped with a triple detector. Both materials afforded classic cylindrical microdomain morphologies in the bulk.[48,49] The molecular characteristics of homopolymers and diblock copolymers used in this study are summarized in Table 1.

Thin Film Preparation. PS-*b*-PFEMS films were prepared by spin-coating 0.25−1.0% w/w polymer solutions in toluene onto single-side polished silicon substrates that were precleaned by repeated toluene rinsing. Solutions were filtered with a Whatman 13 mm GD/X nylon syringe filter (0.45 μm pore size) immediately prior to spin-coating. The ~1 cm^2 Si wafers were coated with the polymer solution and immediately accelerated to 600 rpm for 18 s, followed by 60 s at 1000 rpm. Alternatively, PS-*b*-PFEMS films were prepared by dip-coating from similar toluene solutions to that indicated above. Single-side polished silicon substrates that were precleaned by repeated toluene rinsing or Formvar-coated TEM grids were immersed in the coating solution for 15 s and withdrawn at ~15 cm/s.

Thin Film Annealing. PS-*b*-PFEMS films were annealed by a solvent evaporation procedure.[10] For an unsaturated toluene atmosphere anneal, thin films (~1 cm^2) were placed into a chamber (an inverted 1 L crystallization dish on top of an aluminum foil covered cloth) with a small beaker of toluene (~25 mL) at ambient temperature and pressure. Within 6 h the samples were observed to change color, indicative of the swelling of the film with toluene. After ~24 h the films were removed from the chamber and allowed to dry at ambient conditions for 6 h. Given an air velocity in the annealing chamber of ~0.5 cm/s, an evaporation rate of toluene of ~2.6 g/day, the diameter of 3.1 cm for the toluene vessel, and a relative humidity of less than 1%, we estimate the partial pressure of toluene (P_{Tol}), nitrogen (P_{N_2}), and oxygen (P_{O_2}) as 0.01, 0.77,

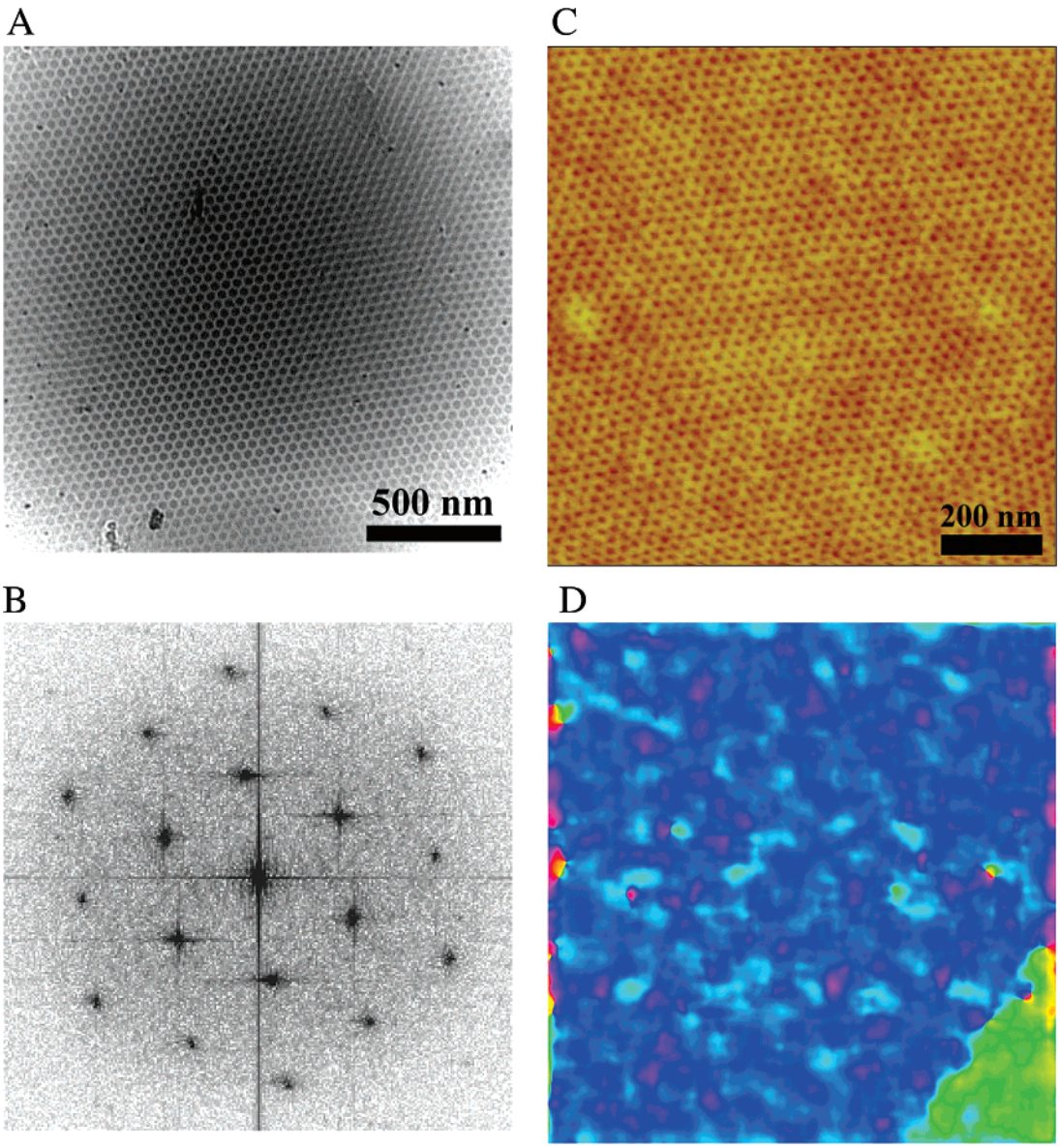

Figure 4. (A) Transmission electron micrograph of toluene evaporation annealed dip coated film of PS-*b*-PFEMS (0.36) (PFEMS areas are dark, whereas PS areas are lighter in the TEM image) and (B) the corresponding 2D Fourier transform. (C) Height image scanning force micrograph of toluene evaporation annealed dip coated film of PS-*b*-PFEMS (0.25) and (D) corresponding color-defined grains obtained from analysis developed by Chaikin, Register, and co-workers.

and 0.22 atm, respectively.[52] Alternatively, for a more aggressive anneal with a saturated toluene atmosphere, a 2 kg mass was placed on top of the chamber so as to increase the quality of the seal with the foil/cloth covered table top, thereby minimizing the exchange between the ambient air and the enclosed toluene vapor-rich atmosphere. After ~24 h the sample was removed from the chamber, where the chamber's surfaces showed condensed toluene droplets (indicative of a near-saturated toluene atmosphere). In this case P_{Tol}, P_{N_2}, and P_{O_2} are 0.04, 0.75, and 0.21 atm, respectively. Drying times were identical to those indicated above. In all cases the film thicknesses were found to be consistent with unannealed precursors as estimated by SFM and ellipsometry. A similar value was determined for an unannealed sample, confirming film stability to the mild annealing conditions.

Contact Angle Measurements. Water contact angles for PS and PFEMS homopolymers were measured using water droplets.[22] A PS homopolymer was acquired from Aldrich, whereas the PFEMS homopolymer was synthesized according to literature procedures.[53] The experimentally determined contact angles for a stationary droplet of water on 100 nm thick PS and PFEMS films were 90 ± 1° and 94 ± 1°, respectively. The contact angles for a stationary droplet of water on the films shown in Figure 2A,B were ~92 ± 1°. Since the contact angle of the PS-*b*-PFEMS is between that of PS and PFEMS homopolymers, then both blocks must be at the surface.

Discussion

Morphology in the As-Cast Thin Films. Thin films (~100 nm) of PS-*b*-PFEMS (0.25) and PS-*b*-PFEMS (0.36) were spin-coated onto silicon wafers from toluene solutions (~1.0% w/w). Shown in Figure 1 are the tapping mode SFM height images. Since the glass transition temperature of PFEMS is near room temperature (~ 16 °C[48,53]), whereas that for PS is ~ 100 °C,[54] the lighter (higher) features can be attributed to PS, while the darker (lower) regions are PFEMS. A disordered cylindrical microdomain morphology is seen with the cylinders oriented parallel to the film surface. This is in agreement with bulk small-angle X-ray scattering data for PS-*b*-PFEMS (0.25) and PS-*b*-PFEMS (0.36).[48,49] These as-cast films were stable at ambient conditions for prolonged periods (up to 1 year) due to the glassy nature of the PS microdomains.

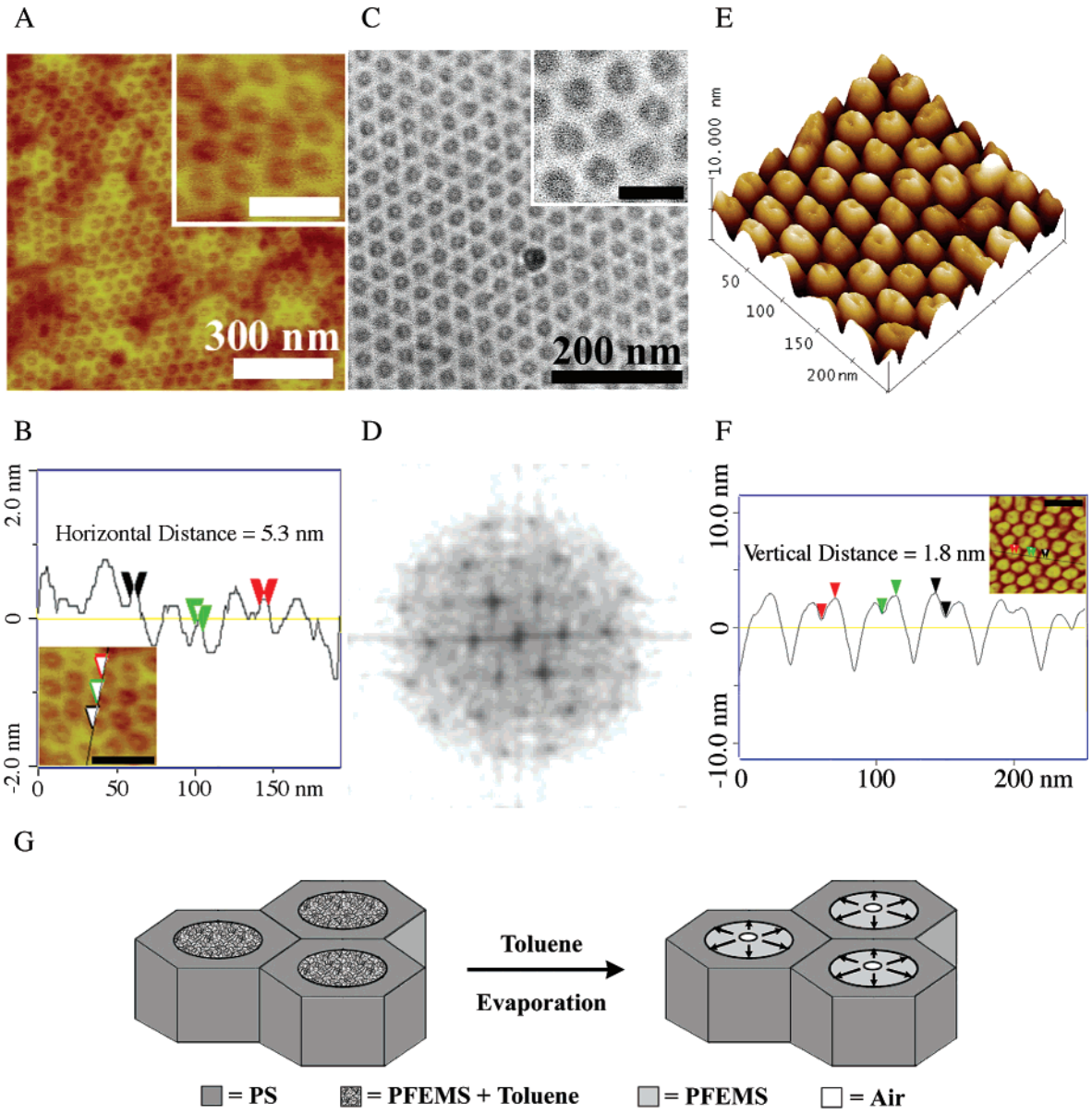

Figure 5. (A) High-resolution height mode SFM images (inset scale bar = 100 nm) of toluene evaporation annealed PS-*b*-PFEMS (0.36) ultrathin film and (B) its cross-sectional analysis. (C) High-resolution TEM images (inset scale bar = 50 nm) of toluene evaporation annealed PS-*b*-PFEMS (0.36) ultrathin film and (D) its 2D Fourier transform. (E) High-resolution SFM image (height mode) of UV ozone treated ultrathin film from (A) and (F) its cross-sectional analysis (inset scale bar = 100 nm). (G) Schematic representing the generation of cylinder centered nanopore from ongoing toluene evaporation once PS lattice is vitrified.

Shown in Figure 2 are the tapping mode SFM height images of the films following an unsaturated toluene atmosphere anneal (see Experimental Section). An ordered, aligned array of cylindrical microdomains mostly oriented parallel to the film surface is seen. No variations in the surface topography, due to the formation of islands and holes, were observed. The solubility parameters of PS and PFEMS are 18.5 and 19.5 $MPa^{1/2}$, respectively.[54−56] The experimentally determined value for the solubility parameter for toluene is 18.2 $MPa^{1/2}$.[54] Consequently, PS is slightly more soluble in toluene than PFEMS. This, in addition to a slight preference of PFEMS to the substrate,[57] forces an orientation of the microdomains parallel to the surface, and, with the enhanced mobility due to the presence of the solvent, highly ordered, highly aligned domains are obtained.

To overcome any preferential interfacial interactions, we increased the concentration of toluene in the films by saturating the annealing chamber (see Experimental Section). After annealing a 100 nm thick film of PS-*b*-PFEMS (0.36) in a toluene-saturated toluene environment, the surface was investigated by SFM (Figure 3A). In this case, the entire film exhibits a highly ordered hexagonal lattice (up to 1.0 μm^2 in area) of cylindrical microdomains oriented normal to the substrate. At this film thickness, a higher concentration of toluene mediates the interfacial interactions sufficiently to obtain a perpendicular orientation at the film−air surface. A 2-dimensional Fourier transform of this height image is shown in Figure 3B. The six sharp first-order reflections, used to determine a periodicity of 42.8 nm, as well as some weaker higher order reflections further confirm the long-range order in the film. This sample was further characterized by small-angle X-ray scattering (SAXS), and for comparison, a plot of the bulk equilibrium SAXS of PS-*b*-PFEMS (0.36) is also included (Figure 3C, black trace and gray traces, respectively). The primary intensity peaks for the thin film ($q^* = 0.017\,55$) and bulk state plots ($q^* = 0.017\,08$) correspond to periodicities of 41.3 and 42.5 nm, respectively. By SAXS, it seems that a slight difference in periodicity exists

between bulk and thin film morphology. Nevertheless, the SAXS-determined periodicity found here agrees well with that from the SFM 2-D Fourier transform data.

Spin-coated PS-*b*-PFEMS films less than 100 nm in thickness dewetted from the substrate during preparation. However, stable films, 12−15 nm in thickness, could be prepared by dip- or drop-coating from dilute solutions. In this case, with the film thickness less than the block copolymer periodicity, only the energetically favorable normal-to-substrate orientation of the morphology was observed when these ultrathin films were annealed using the *unsaturated* toluene environment. Shown in Figure 4A is a representative transmission electron microscopy (TEM) image obtained by dip-coating a TEM grid (similar images were obtained for drop-coated samples). All samples were imaged without staining, since the high electron density associated with the main-chain Fe atoms provided sufficient electron density contrast. The solvent-annealed samples were found to be very well-ordered with a hexagonal lattice of cylindrical microdomains covering areas in excess of 2 μm^2. To further confirm the long range-order observed by TEM, a 2-D Fourier transform was performed on the image in Figure 4A. As shown in Figure 4B, long-range order is verified by sharp 6 first-order and 12 second-order peaks. Subsequently, we applied this technique to the casting and annealing of PS-*b*-PFEMS films on silicon substrates. SFM images of the surface revealed very long-range lateral ordering of the cylindrical microdomais for both PS-*b*-PFEMS (0.25) and PS-*b*-PFEMS (0.36) films. Shown in Figure 4C is a representative SFM height image of a PS-*b*-PFEMS (0.25) film where only a representative fraction of an ordered area that was ~3 μm^2 in area is shown. Using analysis developed by Chaikin, Register, and co-workers, where different colors are assigned to grains having a lattice with a given planar orientation, a color map of Figure 4C was obtained (Figure 4D). With the exception of the edges of the image, a single color is seen within each grain showing that the number of lattice defects per grain is small.

In addition to the long-range order seen in the ultrathin films, examination of the PFEMS cylindrical microdomains by high-resolution SFM and TEM showed a further detail. Shown in Figure 5A are representative high-resolution SFM height images of the toluene-annealed PS-*b*-PFEMS (0.36) ultrathin films. At the center of each cylindrical microdomain there is a well-defined feature ~5.3 nm in diameter. A high-resolution TEM image of this film, shown in Figure 5C, shows that the electron density of this feature is low. From TEM a diameter of ~5 nm is found, consistent with the SFM. As described previously, PFEMS is resistant to UV-ozonolysis whereas PS is readily decomposed and eliminated as volatile carbonaceous compounds. The resulting films consist of hexagonally patterned PFEMS-based amorphous oxides of silicon and iron, as identified previously by X-ray photoelectron spectroscopy.[49] Shown in Figure 5E is a high-resolution SFM image of the ultrathin film after UV ozonolysis. It was found that the PS-based matrix was selectively degraded, and PFEMS cylindrical domains were converted to inorganic oxide. Closer inspection suggests that there is a pore running down the center of each inorganic oxide cylinder or that a ring of oxide has been formed. Fabricating nanoscopic rings has been a challenge, yet here a very simple process has been described to achieve this end. These results suggest that the original morphology consisted of a PS matrix with either PFEMS cylindrical microdomains having central cores of PS or PFEMS cylindrical microdomains bearing empty channels centered along their axes. The former morphology is not expected for a simple diblock copolymer; however, Gido and co-workers have made similar observations on PS-*b*-poly(cyclohexadiene) diblock copolymers.[58] Since the results reported here were obtained on solvent-cast films, the observed morphology cannot be associated with an equilibrium morphology. Therefore, as shown in the schematic (Figure 5), it is possible that during solvent evaporation an enlarged copolymer morphology is frozen in as the T_g of the PS is traversed and further evaporation of the solvent opens a hole in the center of the cylindrical microdomain. Consistent with this is the fact that the average center-to-center distance between the cylindrical microdomains in the bulk is 42.1 nm, where from the SFM images this distance is 45.0 nm. Consequently, a significant increase in the repeat period is seen in the thin films, which suggests the presence of a pore in the center of the microdomains. However, we do not, at present, have a quantitative understanding of the observed morphology, though the result is highly reproducible.[59] Attempts to further anneal these ultrathin films (either using thermal or solvent annealing techniques) unfortunately led to the dewetting of the film from the surface and loss of both the said morphology and order.

Conclusions

In summary, we have shown that PS-*b*-PFEMS diblock copolymers with $\phi_{PFEMS} = 0.25$ and 0.36 self-assemble in thin films to form cylindrical microdomains of PFEMS in a PS matrix. Control over the orientation and long-range ordering can be achieved by judicious control over the solvent evaporation conditions. In addition, in the case of ultrathin films, a novel route for the generation of nanorings is demonstrated where, during solvent evaporation, a pore has been opened in the center of the PFEMS cylindrical microdomains. The facile route to well-ordered arrays of iron-rich nanorings has potential interest in numerous fields such as magnetic data storage where a flux-closure state with zero net magnetic moment exists for ring-like arrays of iron oxide crystals.[60]

Acknowledgment. We are grateful to Jennifer Lu at Agilent Technologies for access to UV ozone etching equipment. Gratitude is extended to Chantal Paquet for ellipsometry measurements. K.A.C. acknowledges funding from Seagate Technology, and T.P.R. acknowledges funding from the Department of Energy, DEF0296ER45612. The authors also thank the NSF MRSEC Shared Experimental Facilities for X-ray scattering measurements. We also acknowledge the Ontario Government for OGSST and OGS Fellowships for D.A.R. In addition, I.M. is grateful to the Canadian Government for a Canada Research Chair and to the European Union for a Marie Curie Research Chair.

References and Notes

(1) Alexandridis, P.; Lindman, B. *Amphiphilic Block Copolymers*; Elsevier: Amsterdam, 2000.
(2) Krausch, G.; Magerle, R. *Adv. Mater.* **2002**, *14*, 1579−1583.
(3) Park, M.; Harrison, C.; Chaikin, P. M.; Register, R. A.; Adamson, D. H. *Science* **1997**, *276*, 1401−1404.
(4) Hamley, I. W. *Angew. Chem., Int. Ed.* **2003**, *42*, 1692−1712.
(5) Matsen, M. W.; Bates, F. S. *Macromolecules* **1996**, *29*, 1091−1098.
(6) Kim, G.; Libera, M. *Macromolecules* **1998**, *31*, 2569−2577.
(7) Kim, G.; Libera, M. *Macromolecules* **1998**, *31*, 2670−2672.
(8) Lin, Z. Q.; Kim, D. H.; Wu, X. D.; Boosahda, L.; Stone, D.; LaRose, L.; Russell, T. P. *Adv. Mater.* **2002**, *14*, 1373−1376.
(9) Temple, K.; Kulbaba, K.; Power-Billard, K. N.; Manners, I.; Leach, K. A.; Xu, T.; Russell, T. P.; Hawker, C. J. *Adv. Mater.* **2003**, *15*, 297−300.
(10) We have preliminarily screened several solvents (chloroform, methylene chloride, tetrahydrofuran, benzene, chlorobenzene, and toluene) for this annealing technique. In terms of ordering our block copolymer thin films over large areas, toluene was the most successful and the

only solvent capable of generating the nanoporous cylindrical morphology. For earlier work on this technique, please refer to: Kim, S. H.; Misner, M. J.; Xu, T.; Kimura, M.; Russell, T. P. *Adv. Mater.* **2004**, *16*, 226−231.
(11) Cavicchi, K. A.; Russell, T. P. *Macromolecules* **2007**, *40*, 1181−1186.
(12) Manners, I. *Synthetic Metal-Containing Polymers*; Wiley-VCH: Weinheim, 2004.
(13) Park, C.; McAlvin, J. E.; Fraser, C. L.; Thomas, E. L. *Chem. Mater.* **2002**, *14*, 1225−1230.
(14) Gohy, J.-F.; Lohmeijer, B. G. G.; Varshney, S. K.; Schubert, U. S. *Macromolecules* **2002**, *35*, 7427−7435.
(15) Hou, S.; Man, K. Y. K.; Chan, W. K. *Langmuir* **2003**, *19*, 2485−2490.
(16) Manners, I. *Science* **2001**, *294*, 1664−1666.
(17) Rulkens, R.; Ni, Y.; Manners, I. *J. Am. Chem. Soc.* **1994**, *116*, 12121−12122.
(18) Ni, Y.; Rulkens, R.; Manners, I. *J. Am. Chem. Soc.* **1996**, *118*, 4102−4114.
(19) Kulbaba, K.; Manners, I. *Macromol. Rapid Commun.* **2001**, *22*, 711−724.
(20) Massey, J. A.; Power, K. N.; Winnik, M. A.; Manners, I. *Adv. Mater.* **1998**, *10*, 1559−1562.
(21) Massey, J. A.; Winnik, M. A.; Manners, I.; Chan, V. Z.-H.; Ostermann, J. M.; Enchelmaier, R.; Spatz, J. P.; Möller, M. *J. Am. Chem. Soc.* **2001**, *123*, 3147−3148.
(22) Raez, J.; Manners, I.; Winnik, M. A. *J. Am. Chem. Soc.* **2002**, *124*, 10381−10395.
(23) Power-Billard, K. N.; Spontak, R. J.; Manners, I. *Angew. Chem., Int. Ed.* **2004**, *43*, 1260−1264.
(24) Korczagin, I.; Hempenius, M. A.; Fokkink, R. G.; Cohen Stuart, M. A.; Al-Hussein, M.; Bomans, P. H. H.; Frederik, P. M.; Vancso, G. J. *Macromolecules* **2006**, *39*, 2306−2315.
(25) Lammertink, R. G. H.; Hempenius, M. A.; Thomas, E. L.; Vancso, G. J. *J. Polym. Sci., Part B: Polym. Phys.* **1999**, *37*, 1009−1021.
(26) (a) Eitouni, H. B.; Balsara, N. P. *J. Am. Chem. Soc.* **2004**, *126*, 7446−7447. (b) Eitouni, H. B.; Balsara, N. P. *J. Am. Chem. Soc.* **2006**, *128*, 16248−16252.
(27) Eitouni, H. B.; Balsara, N. P.; Hahn, H.; Pople, J. A.; Hempenius, M. A. *Macromolecules* **2002**, *35*, 7765−7772.
(28) Kloninger, C.; Rehahn, M. *Macromolecules* **2004**, *37*, 1720−1727.
(29) Li, W.; Sheller, N.; Forster, M. D.; Balaishis, D.; Manners, I.; Annis, I.; Lin, J. S. *Polymer* **2000**, *41*, 719−724.
(30) Manners, I. *Chem. Commun.* **1999**, 857−865.
(31) Datta, U.; Rehahn, M. *Macromol. Rapid Commun.* **2004**, *25*, 1615−1622.
(32) Lastella, S.; Jung, Y. J.; Yang, H.; Vajtai, R.; Ajayan, P. M.; Ryu, C. Y.; Rider, D. A.; Manners, I. *J. Mater. Chem.* **2004**, *14*, 1791−1794.
(33) Hinderling, C.; Keles, Y.; Stöckli, T.; Knapp, H. F.; de los Arcos, T.; Oelhafen, P.; Korczagin, I.; Hempenius, M. A.; Vancso, G. J.; Pugin, R.; Heinzelmann, H. *Adv. Mater.* **2004**, *16*, 876−879.
(34) Cheng, J. Y.; Ross, C. A.; Chan, V. Z.-H.; Thomas, E. L.; Lammertink, R. G. H.; Vancso, J. *Adv. Mater.* **2001**, *13*, 1174−1178.
(35) Rasburn, J.; Petersen, R.; Jahr, T.; Rulkens, R.; Manners, I.; Vancso, G. J. *Chem. Mater.* **1995**, *7*, 871−877.
(36) Lammertink, R. G. H.; Hempenius, M. A.; Manners, I.; Vancso, G. J. *Macromolecules* **1998**, *31*, 795−800.
(37) Papkov, V. S.; Gerasimov, M. V.; Dubovik, I. I.; Sharma, S.; Dementiev, V. V.; Pannell, K. H. *Macromolecules* **2000**, *33*, 7107−7115.
(38) Chen, Z.; Foster, M. D.; Zhuo, W.; Fong, H.; Reneker, D. H.; Resendes, R.; Manners, I. *Macromolecules* **2001**, *34*, 6156−6158.
(39) Hamley, I. W.; Fairclough, J. P. A.; Terrill, N. J.; Ryan, A. J.; Lipic, P. M.; Bates, F. S.; Towns-Andrews, E. *Macromolecules* **1996**, *29*, 8835−8843.
(40) Quiram, D. J.; Register, R. A.; Marchand, G. R.; Ryan, A. J. *Macromolecules* **1997**, *30*, 8338−8343.
(41) Quiram, D. J.; Register, R. A.; Marchand, G. R.; Adamson, D. H. *Macromolecules* **1998**, *31*, 4891−4898.
(42) Massey, J. A.; Temple, K.; Cao, L.; Rharbi, Y.; Raez, J.; Winnik, M. A.; Manners, I. *J. Am. Chem. Soc.* **2000**, *122*, 11577−11584.
(43) Loo, Y.-L.; Register, R. A.; Ryan, A. J. *Phys. Rev. Lett.* **2000**, *84*, 4120−4123.
(44) Li, L.; Séréro, Y.; Koch, M. H. J.; de Jeu, W. H. *Macromolecules* **2003**, *36*, 529−532.
(45) Zhu, L.; Calhoun, B. H.; Ge, Q.; Quirk, R. P.; Cheng, S. Z. D.; Thomas, E. L.; Hsiao, B. S.; Yeh, F.; Liu, L.; Lotz, B. *Macromolecules* **2001**, *34*, 1244−1251.
(46) Zhu, L.; Cheng, S. Z. D.; Calhoun, B. H.; Ge, Q.; Quirk, R. P.; Thomas, E. L.; Hsiao, B. S.; Yeh, F.; Lotz, B. *J. Am. Chem. Soc.* **2000**, *122*, 5957−5967.
(47) Loo, Y.-L.; Register, R. A.; Ryan, A. J. *Macromolecules* **2002**, *35*, 2365−2374.
(48) Rider, D. A.; Cavicchi, K. A.; Power-Billard, K. N.; Russell, T. P.; Manners, I. *Macromolecules* **2005**, *38*, 6931−6938.
(49) Lu, J. Q.; Kopley, T. E.; Moll, N.; Roitman, D.; Chamberlin, D.; Fu, Q.; Liu, J.; Russell, T. P.; Rider, D. A.; Manners, I.; Winnik, M. A. *Chem. Mater.* **2005**, *17*, 2227−2231.
(50) Massey, J. A.; Kulbaba, K.; Winnik, M. A.; Manners, I. *J. Polym. Sci., Part B: Polym. Phys.* **2000**, *38*, 3032−3041.
(51) Paquet, C.; Cyr, P. W.; Kumacheva, E.; Manners, I. *Chem. Mater.* **2004**, *16*, 5205−5211.
(52) Hummel, A. A.; Braun, K. O.; Fehrenbacher, M. C. *Am. Ind. Hygien. Assoc. J.* **1996**, *57*, 519−525.
(53) Temple, K.; Massey, J. A.; Chen, Z.; Vaidya, N.; Berenbaum, A.; Foster, M. D.; Manners, I. *J. Inorg. Organomet. Polym.* **1999**, *9*, 189−198.
(54) *Encyclopedia of Polymer Science and Engineering*, 2nd ed.; John Wiley & Sons: New York, 1987; Vol. 16.
(55) Kulbaba, K.; MacLachlan, M. J.; Evans, C. E. B.; Manners, I. *Macromol. Chem. Phys.* **2001**, *202*, 1768−1775.
(56) Swelling techniques have been used to investigate the ∂_{PFEMS}. Arsenault, A. C.; Míguez, H.; Kitaev, V.; Ozin, G. A.; Manners, I. *Adv. Mater.* **2003**, *15*, 503−507. Additionally, the solubility parameter can be calculated using $\partial_{PFDMS} = 18.7$ MPa$^{1/2}$ and the equation $\partial =$ (polymer density) $\times \sum G/M$, where $\sum G$ is the sum of all group molar attraction constants (G) established by Small and Hoy and M is the repeat unit molecular weight. Small, P. A. *J. Appl. Chem.* **1953**, *3*, 71−80. Hoy, K. L. *J. Paint Technol.* **1970**, *42*, 76−80.
(57) X-ray photoelectron spectroscopy and commensurability arguments have been used to propose that poly(ferrocenyldimethylsilane) has a slight preference for the substrate in polystyrene block copolymers. Lammertink, R. G. H.; Hempenius, M. A.; Vancso, G. J.; Shin, K.; Rafailovich, M. H.; Sokolov, J. *Macromolecules* **2001**, *34*, 942−950.
(58) David, J. L.; Gido, S. P.; Hong, K.; Zhou, J.; Mays, J. W.; Tan, N. B. *Macromolecules* **1999**, *32*, 3216−3226.
(59) (a) Extensive thin film investigations (varied film thickness, varied solvents for solvent annealing, varied annealing conditions) using the other PS-*b*-PFEMS diblock copolymers (including PS-*b*-PFEMS (0.25)) have shown that this nanoporous morphology only arises when PS-*b*-PFEMS (0.36) is used. Although it seems that this morphology is specific to this polymer system, it is certainly possible that these results may be reproduced with a different polymer in the future. (b) Extensive staining experiments using RuO_4 have been conducted in an attempt to confirm this nanoporous cylindrical thin film morphology. Unfortunately, an interesting interfacial staining artifact prevents confirmation of this morphology with complete certainty. See: Wang, Y.; Coombs, N.; Turak, A.; Lu, Z.-H.; Manners, I.; Winnik, M. A. *Macromolecules* **2007**, *40*, 1594−1597.
(60) (a) We have preliminarily shown by magnetic force microscopy that these rings are magnetic. We are currently investigating the nature of the magnetism. Our areal density of magnetic rings = 990 rings/μm^2. For a recently published nanosphere template approach see: Zhu, F. Q.; Fan, D.; Zhu, X.; Zhu, J.-G.; Cammarata, R. C.; Chien, C.-L. *Adv. Mater.* **2004**, *16*, 2155−2159. (b) Tripp, S. L.; Dunin-Borkowski, R. E.; Wei, A. *Angew. Chem., Int. Ed.* **2003**, *42*, 5591−5593.

MA062073U